Eif2b3 mutants recapitulate phenotypes of Vanishing White Matter Disease and validate novel disease alleles in zebrafish

Yu-Ri Lee[1,10], Se Hee Kim[2,10], Afif Ben-Mahmoud[3,10], Oc-Hee Kim[1], Tae-Ik Choi[1], Kang-Han Lee[1], Bonsu Ku[4], Juneyong Eum[5], Yun Kee[5], Sangkyu Lee[6], Jihoon Cha[7], DongJu Won[8], Seung-Tae Lee[8], Jong Rak Choi[8], Joon Soo Lee[2], Heung Dong Kim[2], Hyung-Goo Kim[3,*], Joshua L. Bonkowsky[9,*], Hoon-Chul Kang[2,*], Cheol-Hee Kim[1,*]

[1]*Department of Biology, Chungnam National University, Daejeon, Korea*

[2]*Department of Pediatrics, Division of Pediatric Neurology, Pediatric Epilepsy Clinic, Epilepsy Research Institute, Yonsei University College of Medicine, Severance Children's Hospital, Seoul, Korea*

[3]*Neurological Disorders Research Center, Qatar Biomedical Research Institute, Hamad Bin Khalifa University, Doha, Qatar*

[4]*Korea Research Institute of Bioscience and Biotechnology, Daejeon, Korea*

[5]*Division of Biomedical Convergence, Kangwon National University, Chuncheon, Korea*

[6]*College of Pharmacy, Kyungpook National University, Daegu, Korea*

[7]*Department of Radiology and Research Institute of Radiological Science, Severance Hospital, Yonsei University College of Medicine, Seoul, Korea*

[8]*Department of Laboratory Medicine, Severance Hospital, Yonsei University College of Medicine, Seoul, Korea*

[9]*Department of Pediatrics, University of Utah School of Medicine; Brain and Spine Center, Primary Children's Hospital; Salt Lake City, Utah, USA*

[10]*These authors contributed equally to this work.*

*To whom correspondence should be addressed: Cheol-Hee Kim, Department of Biology, Chungnam National University, 99 Daehak-ro, Yuseong-gu, Daejeon 34134, Korea; Phone: 82-42-821-5494; Fax: 82-42-822-9690; Email: zebrakim@cnu.ac.kr

Abstract

Leukodystrophy with Vanishing White Matter (VWM), also called Childhood Ataxia with Central Nervous System Hypomyelination (CACH), is caused by mutations in the subunits of the eukaryotic translation initiation factor, *EIF2B1*, *EIF2B2*, *EIF2B3*, *EIF2B4*, or *EIF2B5*. However, little is known regarding the underlying pathogenetic mechanisms, and there is no curative treatment for VWM. In this study, we established the first EIF2B3 animal model for VWM disease in vertebrates by CRISPR mutagenesis of the highly conserved zebrafish ortholog *eif2b3*. Using CRISPR, we generated two mutant alleles in zebrafish *eif2b3*, 10- and 16-bp deletions, respectively. The *eif2b3* mutants showed defects in myelin development and glial cell differentiation, and increased expression of genes in the induced stress response pathway. Interestingly, we also found ectopic angiogenesis and increased VEGF expression. Ectopic angiogenesis in the *eif2b3* mutants was reduced by administration of VEGF receptor inhibitor SU5416. Using the *eif2b3* mutant zebrafish model together with *in silico* protein modeling analysis, we demonstrated the pathogenicity of 18 reported mutations in *EIF2B3*, as well as of a novel variant identified in a 19-month-old female patient: c.503T>C (p.Leu168Pro). In summary, our zebrafish mutant model of *eif2b3* provides novel insights into VWM pathogenesis and offers rapid functional analysis of human *EIF2B3* gene variants.

Introduction

Leukodystrophies are a group of chronic disorders that affect white matter of the central nervous system, causing motor and intellectual impairment, and often progressing to early death. One severe leukodystrophy known as vanishing white matter (VWM) disease is an autosomal recessive condition caused by pathogenic mutations in any of the five genes encoding subunits for the eukaryotic translation initiation factor (EIF) 2B: *EIF2B1*, *EIF2B2*, *EIF2B3*, *EIF2B4*, or *EIF2B5* (1). EIF2B functions as a decameric protein composed of two pentamers, each pentamer composed of subunits EIF2B1~5. EIF2B is critical for protein synthesis initiation, and is a guanine nucleotide exchange factor to convert the inactive GDP-bound state to active GTP-bound state in G-protein cycle to drive successive rounds of translation initiation.

The classic childhood onset form of VWM is characterized by chronic progressive neurological deterioration, cerebellar ataxia, optic atrophy, and episodes of acute deterioration that can be precipitated by minor stresses such as viral febrile illness (2). Milder VWM forms include adult onset variants which can manifest with mild ataxia, ovarian failure, and spasticity (3).

Null alleles of mouse knockouts of the *EIF2B* genes displayed lethality, thereby limiting their use for further study of VWM pathogenicity. Mouse knock-in models for VWM disease display a subtle phenotype, including mild motor problems on rotarod and open field tests, such as is seen in the mouse model for Eif2b5 (R132H mutation) (4). Subsequently, other VWM mouse models were generated in Eif2b4 and Eif2b5, which carry point mutations of R191H in *Eif2b5* and R484W in *Eif2b4* (5). Recently, a spontaneous point mutation in *Eif2b5* (I98M) was identified in a mouse strain with a small body, abnormal gait, male and female infertility, epileptic seizures, and a shortened lifespan (6).

In this study, using zebrafish (*Danio rerio*), we established the first EIF2B3 animal model for VWM disease in vertebrates. High homology between zebrafish and human genes favors the use of zebrafish as a suitable model for the analysis of complex neurological and neuropsychiatric diseases (7-9). We observed defects in myelin gene expression and glial cell differentiation in *eif2b3* mutant zebrafish, recapitulating key human phenotypes. Moreover, we have tested the pathogenicity of a novel variant in *EIF2B3*, which we identified in a Korean VWM patient, along with 18 other known recessive mutations, in rescue experiments using the mutant zebrafish. Finally, we performed protein modeling of this novel allele and four other *EIF2B3* alleles to assess their pathogenicity.

Results

eif2b3 is expressed in the proliferating cells in early development

The zebrafish genome harbors a single *eif2b3* ortholog encoding a 453-amino-acid protein, similar in length to the human protein (452 amino acids) and which is highly conserved (80% similarity; Supplementary Material, Figure S1A). To determine the temporal expression patterns of zebrafish *eif2b3*, stage-specific RT-PCR was performed, revealing that zebrafish *eif2b3* transcripts have both maternal and zygotic expression (Supplementary Material, Figure S1B). Whole-mount *in situ* hybridization showed ubiquitous expression prior to and throughout gastrulation in zebrafish embryos; however, at 1 dpf, *eif2b3* expression was detected in a tissue-specific pattern in the somites of trunk region (Supplementary Material, Figure S1C). By 2 dpf, *eif2b3* expression was noted in the tectum, midbrain-hindbrain boundary, eyes, gut, and liver. These restricted expression patterns indicate that *eif2b3* is expressed primarily in proliferating cells during early development.

eif2b3 mutant zebrafish showed relatively normal development up to 3 dpf

To determine the consequences of *eif2b3* mutation, we performed genome editing and identified mutant alleles. We disrupted the highly conserved nucleotidyl transferase domain by injecting Cas9 mRNA and guide RNA targeting *eif2b3* exon 2, screened for mosaic F0 founders, and finally established two mutant alleles (10- and 16-bp deletion; named *eif2b3*^{ck156a} and *eif2b3*^{ck156b}, respectively). The predicted mutations caused a frame-shift with premature termination (Figure 1). We used the 16-bp deletion mutant (*eif2b3*^{ck156a}) for subsequent experiments. *eif2b3*^{ck156a} mutant embryos displayed similar gross morphology compared to WT until ~3 dpf; however, at 5 dpf *eif2b3*^{ck156a} mutant zebrafish showed small eyes and heart edema (Figure 1E) resulting in lethality by ~8 dpf.

Tail coiling movements in eif2b3 mutant zebrafish indicate normal development of early nervous system

The first locomotor activity in zebrafish starts at 17 hpf with spontaneous tail coiling movements. This simple behavior pattern involves the side to side movement of the tail mediated by a central pattern generator (CPG) of motoneurons and interneurons in the spinal cord. In wild-type embryos at 24 hpf, its frequency is approximately 0.5 Hz. We observed a similar tail coiling frequency in *eif2b3* mutant zebrafish, indicating normal development of the early nervous system (Figure 2A). We also examined motoneuron development using the anti-Synaptotagmin 2 antibody (Znp1) and did not detect gross difference in immunohistochemistry pattern between *eif2b3* mutant zebrafish and WT (Figure 2B).

Defects of myelin development in *eif2b3* KO zebrafish

Neuropathological examination in VWM patients shows abnormal morphology of astrocytes and oligodendrocytes in CNS white matter, including an increase in immature astrocytes but reduced

mature astrocytes numbers (10). Thus, it has been postulated that white matter glial astrocytes do not mature properly in VWM and therefore cannot execute their normal function.

To test whether glial cell maturation and myelination are also affected in *eif2b3* KO zebrafish, we examined molecular markers involved in myelin development: MBP, OLIG2, and Nestin. Myelin basic protein (MBP) is important in the myelination of nerves in the nervous system and maintains the correct structure of myelin while interacting with lipids in the myelin membrane. Glial fibrillary acidic protein is expressed in the developing central nervous system in radial glial-like cell primary progenitor cells. Oligodendrocyte transcription factor (OLIG2) is a basic helix-loop-helix transcription factor. OLIG2 promotes the formation of oligodendrocyte precursors and oligodendrocyte differentiation. Nestin is one of the earliest neural progenitor cell markers expressed in dividing cells during the early stages of development in the nervous system. Also as a marker for immature glial astrocytes, upon differentiation, Nestin becomes downregulated and is replaced by cell type-specific markers, e.g. neurofilaments, GFAP, and OLIG2 in the developing CNS (11).

By whole mount *in situ* hybridization, we observed a significant decrease in *mbp* mRNA expression in the nervous system of *eif2b3* zebrafish mutants at 3 dpf (Figure 2, C and D). To visualize myelinating oligodendrocytes in living animals, we outcrossed *eif2b3* mutant zebrafish with the transgenic *mbp-mGFP* line (12) (Figure 2E). We previously established this *Tg(mbp:mgfp)* transgenic strain expressing membrane-targeted green fluorescent protein (mGFP) under the control of the myelin basic protein (*mbp*) promoter (12). We observed severe defects in myelination in *eif2b3* mutant zebrafish compared to WT zebrafish, which was consistent with the decrease in *mbp* gene expression.

Glial and microglial cell differentiation is altered *eif2b3* KO zebrafish

To understand the defects in myelination in *eif2b3* mutant zebrafish, we examined expression of genes involved in glial cell and oligodendrocyte differentiation. We found up-regulation of *nestin* gene

transcription in the forebrain and midbrain regions of mutant zebrafish as early as 2 dpf (Figure 3, A and B). However, expression of the mature glial cell marker *olig2* was down-regulated in mutant zebrafish at 3 dpf (Figure 3C), although its earlier expression was not significantly changed (Supplementary Material, Figure S2). Given that altered differentiation of glial cell types is reported in VWM pathogenesis (10), we examined whether other cell types were also affected in *eif2b3* zebrafish mutants. Interestingly, we detected ectopic appearance of neutral red-positive microglial progenitor cells (13) in the eye as early as at 2 dpf as well as in the midbrain at 3 dpf of *eif2b3* mutants (Figure 3D). It is known that these neutral red-positive cells are microglial progenitor cells which originate from the embryonic yolk sac, then migrate and invade the brain to differentiate into microglia, as is revealed by apolipoprotein-E (apoE) expression (14). Using *apoeb* as a microglial cell marker, we observed a dramatic change in its expression, with many fewer cells in *eif2b3* mutants compared to WT (Figure 3E). Neutral red-positive cells in 3 dpf *eif2b3* mutant zebrafish and *apoe*-positive cells in 3 dpf WT zebrafish indicate different cell populations. This data is similar to that observed in glial cell development in *eif2b3* mutant zebrafish: up-regulation of the early glial progenitor maker (*nestin*) and down-regulation of the late differentiating glial cell marker (*olig2*).

Ectopic angiogenesis in *eif2b3* mutant zebrafish

At the vascular interface, endfeet processes of perivascular astrocytes closely juxtapose cerebral blood vessels to regulate developmental and physiological processes including endothelial cell proliferation and sprouting as well as the formation of the blood-brain barrier (15, 16). Astrocytes, the most abundant glial cell type of the CNS, are morphologically complex and display numerous processes interacting with synapses and blood vessels. We outcrossed the *eif2b3* mutant zebrafish with a *Tg(kdrl:egfp)* transgenic line and visualized vascular development in 3 dpf embryos with endothelial-specific GFP expression. The live 3D SPIM imaging revealed that mutant embryos displayed hyper-branching of cranial blood vessels in the midbrain region compared to wild type (Figure 4, A and B).

Ectopic angiogenesis was also observed in other regions in *eif2b3* mutant zebrafish, such as intersegmental vessels and subintestinal veins (Supplementary Material, Figure S3). To investigate the background mechanism of ectopic angiogenesis, we examined the expression of vascular endothelial growth factor (VEGF) in *eif2b3* mutant zebrafish compared to wild type by whole-mount *in situ* hybridization. VEGF is a signal protein produced by cells that stimulates the formation of blood vessels (17). The zebrafish VEGF gene, *vegfaa*, was upregulated in *eif2b3* mutant zebrafish, especially in the midbrain region where ectopic angiogenesis was most prominent (Figure 4E). However, expression of the other VEGF homologue, *vegfab*, was not changed. To confirm the involvement of VEGF in the process leading to ectopic angiogenesis in *eif2b3* mutants, we treated embryos with VEGF receptor inhibitor SU5416. Inhibition of VEGF signaling in *eif2b3* mutants reduced ectopic angiogenesis in mutant zebrafish (Figure 4F). The results implicate that *eif2b3* is required for proper vascular development, at least in part by modulating VEGF signaling.

ER stress and angiogenesis

Recent studies have shown that endoplasmic reticulum (ER) stress and the unfolded protein response (UPR) pathway plays an important role in the pathogenesis of VWM (18). ER stress, initiated by the accumulation of unfolded or misfolded proteins, activates the UPR pathway. The UPR is a protective mechanism activated by an overload of unfolded or misfolded proteins in the ER. Abnormal activation of the UPR pathway after ER stress may contribute to pathogenesis of VWM. Activation of the UPR pathway in white matter, predominantly in oligodendrocytes and astrocytes, also has been reported in brain tissue of VWM patients by demonstrating upregulation of X-box-binding protein (XBP1) and activating transcription factor-6 (ATF6) protein levels (19). We examined the expression of UPR pathway genes by whole mount *in situ* hybridization analysis of XBP1, ATF4, and ATF6. We found increased expression of all three of these UPR pathway genes in *eif2b3* mutant zebrafish (Supplementary Material, Figure S4). Although the CNS is the most affected organ in VWM disease,

other organs, including the lens, liver, kidney, pancreas, and ovaries, can have disease involvement (1, 20). Consistently, we observed up-regulation of UPR pathway genes specifically in the lens, liver, pancreas, and intestine of *eif2b3* zebrafish mutants. We also found that expression of an apoptosis-related gene, *tp53* (tumor protein p53), overlapped with that of UPR pathway genes in *eif2b3* mutant zebrafish (Supplementary Material, Figure S4D).

Novel EIF2B3 variants identified in a Korean patient with VWM phenotype

We identified a 19-month-old female patient with clinical and MRI features suggesting VWM disease (Figure 5A). Whole exome sequencing was performed, and two novel compound heterozygous variants (c.89T>C, p.Val30Ala in exon 2 and c.503T>C, p.Leu168Pro in exon 5**,** NM_020365.5, NP_065098.1) of unknown significance were detected in *EIF2B3* (Figure 5B). c.89T>C (p.Val30Ala) mutation was also identified in a Korean patient with infantile-onset VWM without functional analysis during the course of this study (21); however, the variant c.503 T>C; p.Leu168Pro had not been described in any other databases. The two residues Valine30 and Leucine168 were found to be highly conserved across species including zebrafish. Three *in silico* protein analyses, Polyphen2, PROVEAN, and MutationTaster indicated that the two identified variants were likely to be damaging.

Six missense variants cause protein misfolding and steric hindrance in molecular modeling

Next, we analyzed the effects on EIF2B3 protein structure of a novel mutation (L168P) and 5 previously reported mutations (V46I, G47E, A87V, R91H, and R225Q) in the *EIF2B3* gene of VWM patients (Figure 6). We focused on mutations in the N-terminal region except for the case of R225Q, given that the C-terminal region of EIF2B3 is unobservable in the cryo-EM structure (PDB code 6CAJ). Critically, structure-based modeling suggested that proline substitution of Leu168 might cause protein misfolding. This mutation might not only lead to loss of contacts with Arg166 and His190,

which contribute to interior folding, but also bring about steric hindrance between the C_δ atom of mutated proline and the main chain carbonyl group of Gly159 (Figure 6B). Molecular modeling of the mutant proteins suggested that other mutations, such as V46I, G47E, A87V, R91H, or R225Q, may also cause intermolecular steric hindrance among the EIF2B subunits which could impair structural integrity (Figure 6C) by loss of interior atomic contacts (Figure 6, D-F).

Functional validation of patient mutations using eif2b3 KO zebrafish

Among the 25 mutations identified from 61 reported human VWM patients (Supplementary Material, Table S2), we assessed 19 missense mutations in zebrafish rescue experiments. Using site-directed mutagenesis, we generated 20 expression vectors for WT *EIF2B3* cDNA and 19 variants identified from VWM patients: p.Gly11Val, p.Leu27Gln, p.Val30Ala, p.Lys33Glu, p.Val46Ile, p.Gly47Glu, p.Ala87Val, p.Arg91His, p.Gln136Pro, p.Leu168Pro, p.Arg225Gln, p.Gln236Glu, p.Arg312Gln, p.Ala322Gly, p.His341Gln, p.Ile346Thr, p.Ser369fs, p.Val398fs, and p.Cys424Gly. For rescue experiments, these synthetic mRNAs transcribed from each expression vector were microinjected into one-cell stage zebrafish embryos and analyzed at 5 dpf.

To test rescue activity of injected mRNAs, recovery for several morphological defects was carefully examined; for example, swim bladder inflation, yolk absorption, heart edema, eye size, etc. Overexpression of wild-type of human EIF2B3 rescued most of these phenotypes, except for swim bladder inflation. None of the patient-derived EIF2B3 mutation variants, including the novel patient variant, rescued the morphological phenotypes of *eif2b3* mutant zebrafish (Figure 7; Supplementary Material, Figure S5). These results provide the first genetic evidence that the 19 identified *EIF2B3* missense mutations are pathogenic. Additionally, the *eif2b3* zebrafish model demonstrates application as an *in vivo* tool for the rapid functional validation of novel EIF2B3 variants newly identified in VWM patients.

Discussion

VWM disease is one of the most prevalent white matter genetic disorders in childhood (6). It was initially recognized as a devastating brain disorder affecting young children (2); however, it has become apparent that the disease has wide phenotypic variation and may affect people of all ages (10). VWM severity stretches from the moderate type in late childhood-onset to the severe form in congenital or early-childhood onset. The clinical course of VWM is of slow chronic progression, often with intermittent episodes of rapid neurological deterioration that can be provoked by minor stressors, such as mild head trauma or infection accompanied by fever (2). The pathophysiology of VWM, however, is poorly understood and this lack of insight has delayed development of therapeutic treatments. VWM disease is caused by mutations in any of the five EIF2B subunits.

In this study, we generated the first animal model for EIF2B3 mutation causing VWM. Using the small vertebrate model zebrafish, we showed that mutations in zebrafish *eif2b3* phenocopy key aspects of human VWM disease, and demonstrate alterations in glial cell and microglial cell differentiation. Interestingly, we also found ectopic abnormal hyper-branching of blood vessels with increased level of VEGF expression.

Our results provide several novel insights into VWM pathophysiology. First, we found ectopic angiogenesis and increased VEGF expression in mutant zebrafish. Interestingly, other demyelinating disorders also have abnormal angiogenesis. Multiple sclerosis has angiogenesis in demyelinating lesions which are associated with expression of VEGF and several other angiogenic molecules (17, 22). Pathophysiology of cerebral adrenoleukodystrophy has also recently been found to involve endothelial cell dysfunction and abnormal VEGF signaling (23). Another group of leukodystrophies

caused by mutations in aminoacyl-tRNA synthetase proteins (HARS, IARS, TARS, and SARS) (24, 25), were independently identified from large-scale genetic screens for genes important for vascular development in zebrafish (26-28).

Second, we found that *EIF2B3* is required for myelination at early stages of CNS development. The expression of MBP is crucial for the formation of functional myelin sheaths within the CNS (12). We also found alterations in cell differentiation in *eif2b3* mutants: early markers for immature glial cell or microglial cells, *nestin*- or neutral red-positive, showed increased levels of expression; but, inversely, markers of late mature cell types, *olig2* or *apoe*, demonstrated decreased expression. In the CNS, *apoe* gene products are detected in the fibrous astrocytes of white matter, Bergmann glia of the cerebellum, and Muller cells of the retina. Interestingly, in recent studies on VWM patients and mouse models, it was reported that absence or translocation of Bergmann glia is associated with hypomyelination, suggesting Bergmann glia as a novel disease marker for VWM (6, 29). Thus, further studies are required to understand the differentiation of *apoe*-expressing cells and their exact roles during myelination in *eif2b3* mutants.

Lastly, our identification of increased UPR gene expression in *eif2b3* mutants suggested insights into white matter pathology. It is well known that activation of the UPR in response to hypoxia preserves cell viability. For example, hypoxia predominantly affects oligodendrocyte progenitor cells in hypoxia-induced perinatal white matter injury (PWMI), inhibiting their ability to differentiate into myelinating oligodendrocytes which results in myelin loss (30). Myelin-forming cells of the central and peripheral nervous systems (oligodendrocytes and Schwann cells) require the production of a large amount of myelin proteins and lipid-rich membranes; thus, they are particularly susceptible to ER stress. Cells respond to ER stress by activating the UPR which is initially protective, but in situations of prolonged unresolved stress, the UPR can lead to apoptotic death of the cell. There is

evidence that ER stress and the UPR play a role in a number of disorders involving myelin and myelinating glia, including VWM. These data support the idea that abnormal angiogenesis via the UPR pathway and VEGF induction could directly or indirectly affect neurogenesis, oligodendrocyte maturation, and myelination; and thus contribute to VWM pathogenesis. In the mouse brain, VEGF and several factors are secreted in relatively large amounts by neural progenitor cells (NPC), suggesting that NPC may not only be regulated by microglia, but may also be capable of regulating microglial function and activity (31).

Our study also identified and validated a novel VWM *EIF2B3* allele from a patient of Korean ancestry. We diagnosed a 19-month-old Korean female infant with early onset VWM who had a novel compound heterozygous mutations including a novel missense mutation Leu168Pro, and a previously reported missense mutation Val30Ala. Val30Ala and Gln236Glu have been reported in a 20-month-old Korean female baby with infantile-onset VWM (21). We have demonstrated that Val30Ala has a loss-of-function phenotype. The two other variants (Gln236Glu and Leu168Pro) found in Korean infants with VWM, have also been shown to be loss-of-function.

Our work establishes a novel vertebrate model of *EIF2B3*-related VWM disease, demonstrates that the *eif2b3* model is applicable to the rapid functional analysis of EIF2B3 variants, and can serve as a tool for further characterization of the molecular mechanisms underlying VWM disease from which therapeutic approaches may be developed.

Materials and Methods

Case report

Written informed consent was obtained for the patient and this study was approved by the Institutional Review Boards of Severance Hospital (4−2018-0021).

A 19-month-old female infant presented to the emergency room with acute loss of balance and coordination, and rapid regression of her development. Parents reported an upper respiratory infection with fever four days prior to the visit, following which she lost the ability to sit, hold objects, or speak. Her prior medical history was unremarkable: she was born at term following an unremarkable pregnancy via caesarian section to healthy non-consanguineous parents of Korean ancestry. However, her developmental milestones were mildly delayed – she rolled over at 9 months, sat with arm support at 9 months, crawled at 13 months, stood with holding at 12 months, and cruised around furniture at 19 months. She had not achieved standing unassisted or walking. She could only speak 3 words by the age of 19 months. On examination, her Glasgow coma scale score was 8 (E2V2M4). Neurologic examination revealed brisk deep tendon reflexes, extensor plantar responses, and ataxia. A brain MRI showed diffuse T2 hyperintensities of the periventricular and deep white matter with relative sparing of subcortical U-fibers (Figure 6A). By one week after her admission she had become more alert and her Glasgow coma scale score improved to 13 (E4V4M5). At her most recent visit, at age 25 months, she was delayed in her motor and language skills. She could not control her head, roll over, sit, or stand with assist. She could not speak, and could only make incomprehensible sounds.

Clinical exome sequencing

Clinical exome sequencing was performed at Severance Hospital as described previously (32). Genomic DNA samples of the proband underwent panel sequencing to screen 4503 genes using the customized xGen Inherited Diseases Panel (Integrated DNA Technologies, USA). The panel enables deeper sequencing of genomic regions containing genes and SNPs associated with inherited diseases. Two novel compound heterozygous variants (c.89T>C, c.503T>C; p.Val30Ala, p.Leu168Pro) of

unknown significance were detected in *EIF2B3*. *EIF2B3* variants have been deposited in the ClinVar database under accession numbers VCV000617677.2 and VCV000972716.1.

Generation of *eif2b3* mutant zebrafish

To identify the EIF2B3 zebrafish ortholog, we performed reciprocal BLAST of human EIF2B3 protein (Ensembl ID: ENST00000360403.7) against the zebrafish genome and identified a single ortholog with 80% similarity and 63% identity (ENSDART00000184618.1). To understand the *in vivo* role of EIF2B3, we established a zebrafish knockout model utilizing the CRISPR/Cas9 system, as described previously (9). *eif2b3* target sites of CRISPR single guide (sg) RNA and Cas9 were identified using Optimized CRISPR Design (http://crispr.mit.edu/), and selected oligonucleotides were cloned into pDR274 (Addgene) linearized with BsaI (BioLabs).

The templates for in vitro transcription of sgRNAs were produced by PCR using primer 5'-GGGGTGCTGATGGCAGCCGG-3'. In vitro transcription was carried out using 150-200 ng of template and the MaxiScript T7 Kit (Ambion). RNA was precipitated with isopropanol. Cas9 expression vector (Addgene) was linearized with Dra I (Takara) and purified with an agarose gel DNA extraction kit (ELPIS). Cas9 mRNA was transcribed with the mMESSAGE mMACHINE T7 Kit (Ambion), poly (A) tailed with E. coli Poly (A) Polymerase (NEB), and then purified by lithium chloride precipitation following manufacturer protocol.

One-cell stage zebrafish embryos were injected with 300 ng/μl Cas9 mRNA and 150 ng/μl sgRNA. PCR primers for genotyping of *eif2b3* KO mutants were forward primer, 5'-TGTTCGGGATGGAGCTACAG-3', and reverse primer, 5'-CTTCAAATCCCACTCTCTCC-3'. PCR products (20 μl) were re-annealed in a thermal cycler under the following conditions: 95°C for 2 min, 95°C to 85°C at 2°C/s, 85°C to 25°C at 0.1°C/s, then kept at 4°C. 16 μl of the re-annealed mixture was incubated with 0.2 μl of T7 endonuclease I, 2 μl of NEB buffer 2, and 1.8 μl of nuclease-free

water at 37°C for 40 min. To screen for F2 homozygous mutants, PCR was performed using forward primer, 5'-TGTTCGGGATGGAGCTACAG-3', and reverse primer, 5' -TTTGTTGCCCACAGGAAGCA-3'.

Whole-mount *in situ* hybridization

Whole-mount *in situ* hybridization (WISH) was performed essentially as described previously (9). WISH was performed using probes for *eif2b3*, *nestin*, *gfap*, *olig2*, *mbp*, *shha*, *xbp1*, *atf6*, *atf4*, *tp53*, *apoeb*, *vegfaa* and *vegfab*. Briefly, staged embryos were fixed overnight in 4% PFA, then dehydrated in a methanol gradient. Embryos were then rehydrated in phosphate buffered saline containing 0.1% Tween-20 (PBST). Embryos were permeabilized by proteinase K digestion and then hybridized with digoxin-labeled probes overnight at 70°C. The next day, embryos were washed in a preheated mixture of 50% saline sodium citrate containing 0.1% Tween-20 and 50% hybridization solution at 70°C. Embryos were washed again at room temperature and incubated in staining solution in the dark until sufficient staining appeared. Embryos were mounted in glycerol and were visualized using a Nikon AZ100 microscope (Nikon). Images were captured using a Nikon DIGITAL SIGHT DS-Fil1 digital camera (Nikon) and processed with NIS-Elements F 3.0 (Nikon).

Live 3D microscopy of vascular development in zebrafish embryos

To visualize vascular development in zebrafish, *eif2b3*$^{ck15a6/+}$ mutants were crossed with a transgenic *Tg(kdrl:egfp)* line which labels vascular endothelial cells in green (33). Embryonic vasculature was visualized by live 3D selective plane illumination microscopy (SPIM), using a Lightsheet Z.1 fluorescence microscope (Carl Zeiss AG). Each 3 dpf embryo was anesthetized in E3 media containing 0.02% tricaine and embedded within a glass capillary tube (1.0 mm I.D.; Carl Zeiss AG) filled with 1.5% low-melting point agarose in the same medium. The rostral portion of the embryo

was extruded from the capillary and imaged in the imaging chamber filled with E3 media/0.02% tricaine at 27°C throughout the imaging period. A Lightsheet Z.1 fluorescence microscope was equipped with an objective lens (W Plan-Apochromat 20X /1.0 UV-VIS_4909000119) to collect data from 3D imaging. GFP fluorescence was excited with 488 nm lasers and emission was detected by 490 nm Iongpass (LP) filters. The raw data acquired from SPIM imaging were processed with ZEN software v3.0 (Carl Zeiss AG) and optical sections were merged for each z-stack by maximum intensity projection.

To examine the effect of VEGFR inhibitor, zebrafish embryos were treated with 2 μM SU5416 (Sigma) from 26 to 72 hours post-fertilization (hpf). As a control, embryos from the same batch were treated with DMSO at the same concentration (0.1%).

Construction of EIF2B3 allele expression vectors

To generate expression vectors for WT EIF2B3 and the 19 variant alleles identified from VWM patients, we introduced point mutations using site-directed mutagenesis into human EIF2B3 cDNA (Supplementary Material, Table S1, NP_065098.1): p.Leu168Pro (this study), p.Val30Ala, p.Gln236Glu (21), p.Gly11Val, p.Arg312Gln, p.Ala322Gly, p.Ser369fs (34), p.Leu27Gln (35), p.Lys33Glu (36), p.Gly47Glu, p.Ile346Thr (37), p.Ala87Val, p.Arg225Gln, p.Val398fs (20), p.Arg91His (3), p.Val46Ile, p.Gln136Pro, p.His341Gln (1), p.Ser14Phe, p.Ala87Val, p.Ala202Thr, p.Arg438X (38), p.Asp81Asp (39) and p.Cys424Gly (40). Each point mutation was introduced into the WT EIF2B3 expression vector using specific primers in a PCR protocol that amplified the entire plasmid template. PCR was performed using *Pfu* Turbo DNA polymerase (NEB) with denaturation at 95°C for 5 min; 12 cycles of reaction at 95°C for 30 sec, annealing at 55°C for 1 min and extension at 68°C for 11 min and 72°C for 10 min. The parent template was removed using a methylation-dependent endonuclease, Dpn I (NEB). Plasmids were isolated from resulting colonies and screened

for the desired modification. Each mutant construct was sequenced to confirm the desired modification and specific nucleotide substitutions.

Microinjection of synthetic mRNAs for rescue experiments

For rescue experiments, human wild-type and 19 variants including 1 novel variant were tested. Synthetic capped mRNAs were transcribed via the mMESSAGE mMACHINE SP6 Transcription kit (ThermoFisher) using the linearized plasmid DNA as a template. We used the multipurpose pCS2+ expression vector. Synthetic mRNAs were dissolved in 0.2 M KCl with 0.2% phenol red as a tracking dye, then microinjected into one-cell stage zebrafish embryos using a PV820 Pneumatic PicoPump (WPI).

Zebrafish husbandry

Animal experiments were conducted according to approved guidelines and regulations of the Institutional Animal Care and Use Committee (IACUC) at the Animal Ethics Committee of Chungnam National University (CNU-00866). Adult fish were reared under standard conditions with a 14h/10h light/dark cycle. We obtained embryos by natural mating and zebrafish were reared in egg water at 28.5°C. WT zebrafish were obtained from the Zebrafish Center for Disease Modeling (ZCDM).

Spontaneous coiling in embryos

We examined the coiling dynamics during development by assessing spontaneous coiling in unhatched WT and *eif2b3* KO mutant. At 24 hpf, 24 embryos were recorded for 1 min on a stereoscope (S6E, Leica), followed by genotyping.

Supplementary Material

Supplementary Material is available at HMG online.

Acknowledgements

This work was supported by grants from the National Research Foundation (NRF) of Korea (2018M3A9B8021980, 2020R1A5A8017671).

Conflict of Interest Statement. None declared.

References

1 Fogli, A., Schiffmann, R., Bertini, E., Ughetto, S., Combes, P., Eymard-Pierre, E., Kaneski, C.R., Pineda, M., Troncoso, M., Uziel, G. *et al.* (2004) The effect of genotype on the natural history of eIF2B-related leukodystrophies. *Neurology*, **62**, 1509-1517.

2 van der Knaap, M.S., Kamphorst, W., Barth, P.G., Kraaijeveld, C.L., Gut, E. and Valk, J. (1998) Phenotypic variation in leukoencephalopathy with vanishing white matter. *Neurology*, **51**, 540-547.

3 La Piana, R., Vanderver, A., van der Knaap, M., Roux, L., Tampieri, D., Brais, B. and Bernard, G. (2012) Adult-onset vanishing white matter disease due to a novel EIF2B3 mutation. *Arch. Neurol.*, **69**, 765-768.

4 Geva, M., Cabilly, Y., Assaf, Y., Mindroul, N., Marom, L., Raini, G., Pinchasi, D. and Elroy-Stein, O. (2010) A mouse model for eukaryotic translation initiation factor 2B-leucodystrophy reveals abnormal development of brain white matter. *Brain*, **133**, 2448-2461.

5 Dooves, S., Bugiani, M., Postma, N.L., Polder, E., Land, N., Horan, S.T., van Deijk, A.L., van de Kreeke, A., Jacobs, G., Vuong, C. *et al.* (2016) Astrocytes are central in the pathomechanisms of vanishing white matter. *J. Clin. Invest.*, **126**, 1512-1524.

6 Terumitsu-Tsujita, M., Kitaura, H., Miura, I., Kiyama, Y., Goto, F., Muraki, Y., Ominato, S., Hara, N., Simankova, A., Bizen, N. *et al.* (2020) Glial pathology in a novel spontaneous mutant mouse of the Eif2b5 gene: a vanishing white matter disease model. *J. Neurochem.*, **154**, 25-40.

7 May, M., Hwang, K.S., Miles, J., Williams, C., Niranjan, T., Kahler, S.G., Chiurazzi, P., Steindl, K., Van Der Spek, P.J., Swagemakers, S. *et al.* (2015) ZC4H2, an XLID gene, is required for the generation of a specific subset of CNS interneurons. *Hum. Mol. Genet.*, **24**, 4848-4861.

8 Choi, J.H., Jeong, Y.M., Kim, S., Lee, B., Ariyasiri, K., Kim, H.T., Jung, S.H., Hwang, K.S., Choi, T.I., Park, C.O. *et al.* (2018) Targeted knockout of a chemokine-like gene increases anxiety and fear responses. *Proc. Natl. Acad. Sci. U. S. A.*, **115**, E1041-E1050.

9 Lee, Y.R., Khan, K., Armfield-Uhas, K., Srikanth, S., Thompson, N.A., Pardo, M., Yu, L., Norris, J.W., Peng, Y., Gripp, K.W. *et al.* (2020) Mutations in FAM50A suggest that Armfield XLID syndrome is a spliceosomopathy. *Nat. Commun.*, **11**, 3698.

10 Bugiani, M., Boor, I., van Kollenburg, B., Postma, N., Polder, E., van Berkel, C., van Kesteren, R.E., Windrem, M.S., Hol, E.M., Scheper, G.C. *et al.* (2011) Defective glial maturation in vanishing white matter disease. *J. Neuropathol. Exp. Neurol.*, **70**, 69-82.

11 Lendahl, U., Zimmerman, L.B. and McKay, R.D. (1990) CNS stem cells express a new class of intermediate filament protein. *Cell*, **60**, 585-595.

12 Jung, S.H., Kim, S., Chung, A.Y., Kim, H.T., So, J.H., Ryu, J., Park, H.C. and Kim, C.H. (2010) Visualization of myelination in GFP-transgenic zebrafish. *Dev. Dyn.*, **239**, 592-597.

13 Herbomel, P., Thisse, B. and Thisse, C. (2001) Zebrafish early macrophages colonize cephalic mesenchyme and developing brain, retina, and epidermis through a M-CSF receptor-dependent invasive process. *Dev. Biol.*, **238**, 274-288.

14 Rossi, F., Casano, A.M., Henke, K., Richter, K. and Peri, F. (2015) The SLC7A7 Transporter Identifies Microglial Precursors prior to Entry into the Brain. *Cell Rep.*, **11**, 1008-1017.

15 Garden, G.A. and Campbell, B.M. (2016) Glial biomarkers in human central nervous system disease. *Glia*, **64**, 1755-1771.

16 Lundgaard, I., Osorio, M.J., Kress, B.T., Sanggaard, S. and Nedergaard, M. (2014) White matter astrocytes in health and disease. *Neuroscience*, **276**, 161-173.

17 Girolamo, F., Coppola, C., Ribatti, D. and Trojano, M. (2014) Angiogenesis in multiple sclerosis and experimental autoimmune encephalomyelitis. *Acta Neuropathol. Commun.*, **2**, 84.

18 Lin, W. and Popko, B. (2009) Endoplasmic reticulum stress in disorders of myelinating cells. *Nat. Neurosci.*, **12**, 379-385.

19 van Kollenburg, B., van Dijk, J., Garbern, J., Thomas, A.A., Scheper, G.C., Powers, J.M. and van der Knaap, M.S. (2006) Glia-specific activation of all pathways of the unfolded protein response in vanishing white matter disease. *J. Neuropathol. Exp. Neurol.*, **65**, 707-715.

20 van der Knaap, M.S., Leegwater, P.A., Konst, A.A., Visser, A., Naidu, S., Oudejans, C.B., Schutgens, R.B. and Pronk, J.C. (2002) Mutations in each of the five subunits of translation initiation factor eIF2B can cause leukoencephalopathy with vanishing white matter. *Ann. Neurol.*, **51**, 264-270.

21 Hyun, S.E., Choi, B.S., Jang, J.H., Jeon, I., Jang, D.H. and Ryu, J.S. (2019) Correlation Between Vanishing White Matter Disease and Novel Heterozygous EIF2B3 Variants Using Next-Generation Sequencing: A Case Report. *Ann. Rehabil. Med.*, **43**, 234-238.

22 Chapouly, C., Tadesse Argaw, A., Horng, S., Castro, K., Zhang, J., Asp, L., Loo, H., Laitman, B.M., Mariani, J.N., Straus Farber, R. *et al.* (2015) Astrocytic TYMP and VEGFA drive blood-brain barrier opening in inflammatory central nervous system lesions. *Brain*, **138**, 1548-1567.

23 Musolino, P.L., Gong, Y., Snyder, J.M., Jimenez, S., Lok, J., Lo, E.H., Moser, A.B., Grabowski, E.F., Frosch, M.P. and Eichler, F.S. (2015) Brain endothelial dysfunction in cerebral adrenoleukodystrophy. *Brain*, **138**, 3206-3220.

24 Simons, C., Griffin, L.B., Helman, G., Golas, G., Pizzino, A., Bloom, M., Murphy, J.L., Crawford, J., Evans, S.H., Topper, S. *et al.* (2015) Loss-of-function alanyl-tRNA synthetase mutations cause an autosomal-recessive early-onset epileptic encephalopathy with persistent myelination defect. *Am. J. Hum. Genet.*, **96**, 675-681.

25 Fine, A.S., Nemeth, C.L., Kaufman, M.L. and Fatemi, A. (2019) Mitochondrial aminoacyl-tRNA synthetase disorders: an emerging group of developmental disorders of myelination. *J. Neurodev. Disord.*, **11**, 29.

26 Herzog, W., Muller, K., Huisken, J. and Stainier, D.Y. (2009) Genetic evidence for a noncanonical function of seryl-tRNA synthetase in vascular development. *Circ. Res.*, **104**, 1260-1266.

27 Fukui, H., Hanaoka, R. and Kawahara, A. (2009) Noncanonical activity of seryl-tRNA synthetase is involved in vascular development. *Circ. Res.*, **104**, 1253-1259.

28 Castranova, D., Davis, A.E., Lo, B.D., Miller, M.F., Paukstelis, P.J., Swift, M.R., Pham, V.N., Torres-Vazquez, J., Bell, K., Shaw, K.M. *et al.* (2016) Aminoacyl-Transfer RNA Synthetase Deficiency Promotes Angiogenesis via the Unfolded Protein Response Pathway. *Arterioscler. Thromb.*

Vasc. Biol., **36**, 655-662.

29 Dooves, S., Bugiani, M., Wisse, L.E., Abbink, T.E.M., van der Knaap, M.S. and Heine, V.M. (2018) Bergmann glia translocation: a new disease marker for vanishing white matter identifies therapeutic effects of Guanabenz treatment. *Neuropathol. Appl. Neurobiol.*, **44**, 391-403.

30 Volpe, J.J. (2009) Brain injury in premature infants: a complex amalgam of destructive and developmental disturbances. *Lancet Neurol.*, **8**, 110-124.

31 Mosher, K.I., Andres, R.H., Fukuhara, T., Bieri, G., Hasegawa-Moriyama, M., He, Y., Guzman, R. and Wyss-Coray, T. (2012) Neural progenitor cells regulate microglia functions and activity. *Nat. Neurosci.*, **15**, 1485-1487.

32 Kim, S.H., Kim, B., Lee, J.S., Kim, H.D., Choi, J.R., Lee, S.T. and Kang, H.C. (2019) Proband-Only Clinical Exome Sequencing for Neurodevelopmental Disabilities. *Pediatr. Neurol.*, **99**, 47-54.

33 Beis, D., Bartman, T., Jin, S.W., Scott, I.C., D'Amico, L.A., Ober, E.A., Verkade, H., Frantsve, J., Field, H.A., Wehman, A. *et al.* (2005) Genetic and cellular analyses of zebrafish atrioventricular cushion and valve development. *Development*, **132**, 4193-4204.

34 Zhang, H., Dai, L., Chen, N., Zang, L., Leng, X., Du, L., Wang, J., Jiang, Y., Zhang, F., Wu, X. *et al.* (2015) Fifteen novel EIF2B1-5 mutations identified in Chinese children with leukoencephalopathy with vanishing white matter and a long term follow-up. *PLoS One*, **10**, e0118001.

35 Matsukawa, T., Wang, X., Liu, R., Wortham, N.C., Onuki, Y., Kubota, A., Hida, A., Kowa, H., Fukuda, Y., Ishiura, H. *et al.* (2011) Adult-onset leukoencephalopathies with vanishing white matter with novel missense mutations in EIF2B2, EIF2B3, and EIF2B5. *Neurogenetics*, **12**, 259-261.

36 Song, H., Haeri, S., Vogel, H., van der Knaap, M. and Van Haren, K. (2017) Postmortem Whole Exome Sequencing Identifies Novel EIF2B3 Mutation With Prenatal Phenotype in 2 Siblings. *J. Child Neurol.*, **32**, 867-870.

37 Wu, Y., Pan, Y., Du, L., Wang, J., Gu, Q., Gao, Z., Li, J., Leng, X., Qin, J., Wu, X. *et al.*

(2009) Identification of novel EIF2B mutations in Chinese patients with vanishing white matter disease. *J. Hum. Genet.*, **54**, 74-77.

38 Horzinski, L., Huyghe, A., Cardoso, M.C., Gonthier, C., Ouchchane, L., Schiffmann, R., Blanc, P., Boespflug-Tanguy, O. and Fogli, A. (2009) Eukaryotic initiation factor 2B (eIF2B) GEF activity as a diagnostic tool for EIF2B-related disorders. *PLoS One*, **4**, e8318.

39 Perfetto, F., Stoppino, L.P., Cali, A., Milillo, P., Grilli, G., Vinci, R. and Macarini, L. (2012) Childhood Ataxia with Cerebral Hypomyelination Syndrome: a Variant of Patient with Early Childhood Onset Related to EIF2B3 Mutation. A Case Report. *Neuroradiol. J.*, **25**, 81-84.

40 Gowda, V.K., Srinivasan, V.M., Bhat, M. and Benakappa, A. (2017) Case of Childhood Ataxia with Central Nervous System Hypomyelination with a Novel Mutation in EIF2B3 gene. *J. Pediatr. Neurosci.*, **12**, 196-198.

Legends to Figures

Figure 1

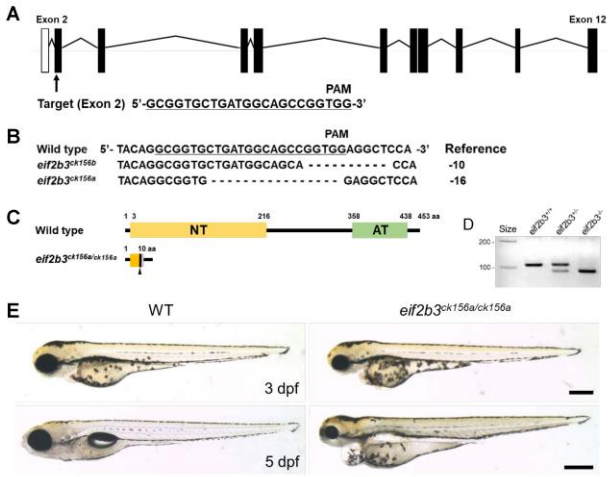

Figure 1. Generation of *eif2b3* mutant zebrafish. (A) Schematic showing the genomic structure of zebrafish *eif2b3* and CRISPR-Cas9 target site in exon 2. Black boxes, coding regions; white box, untranslated region; black lines, introns. (B) Targeted sequence for wild type (WT) and 10- and 16-bp deletion mutants (named *eif2b3*^{ck156a} and *eif2b3*^{ck156b}, respectively). (C) Predicted structure of WT and *eif2b3*^{ck156a} mutant protein. The 16-bp deletion resulted in a frameshift mutation with premature termination. NT; nucleotidyl transferase domain, AT; acyltransferase domain. (D) Agarose gel image of PCR products used to genotype *eif2b3* 16-bp deletion mutant zebrafish embryos. (E) Representative bright field images of WT and *eif2b3* mutant zebrafish at 3 and 5 dpf, respectively. *eif2b3* homozygous mutants show relatively normal development at 3 dpf, but show defects at 5 dpf with small eyes and heart edema compared to WT. Scale bars, 400 μm.

Figure 2

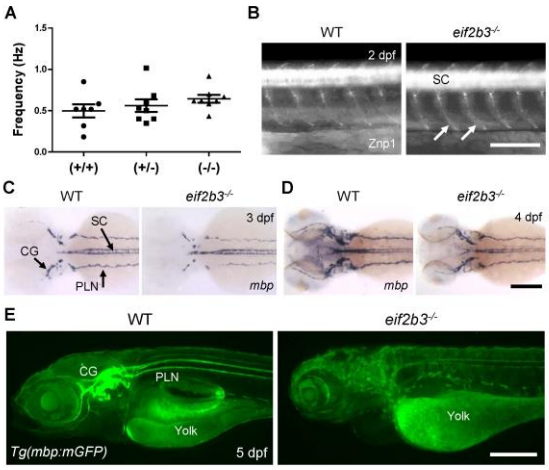

Figure 2. Myelination defects in *eif2b3* mutant zebrafish. (A) Early locomotor activity of *eif2b3* mutant embryos at 1 dpf. No difference in coiling frequency (Hz) of WT, *eif2b3*$^{ck156a/+}$ and *eif2b3*$^{ck156a/ck156a}$ was observed. (B) Motoneuron development appeared normal in *eif2b3* mutant zebrafish at 2 dpf. Scale bar, 100 μm. Whole-mount immunostaining with anti-Synaptotagmin 2 (Znp1). Arrows indicate growing neuronal axons. (C, D) Whole-mount *in situ* hybridization with myelin development marker, *mbp*, in *eif2b3* mutant zebrafish at 3 and 4 dpf. *mbp* expression was reduced in the cranial ganglia (CG) and posterior lateral line nerves (PLN) in *eif2b3* mutant zebrafish compared to WT. Scale bar, 200 μm. (E) Visualization of myelination in live animals using *Tg(mbp:mGFP)* crossed with *eif2b3* mutant zebrafish at 5 dpf. Development of myelination was severely affected in both the CG and PLN in *eif2b3* mutant zebrafish compared to WT. Autofluorescence was also observed in the yolk and eyes. Scale bar, 200 μm.

Figure 3

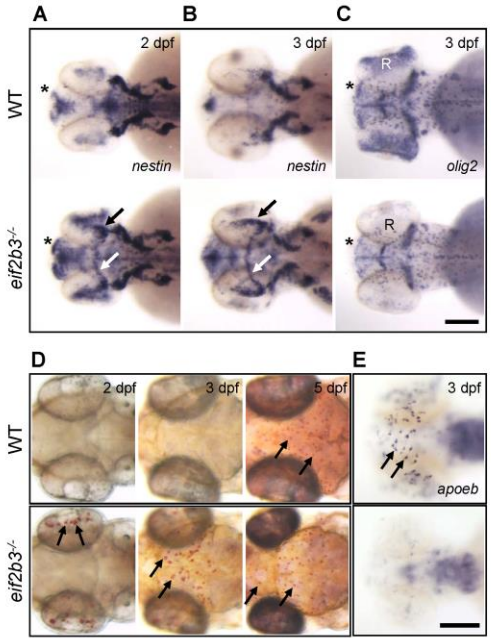

Figure 3. Alteration of cell fates in glial and microglial progenitor cells. (A, B) Early immature glial cell marker, *nestin*, was ectopically expressed in *eif2b3* mutant zebrafish, as early as 2 dpf. Its ectopic appearance was prominent in the forebrain (asterisk) and midbrain (arrows) regions, compared to WT. (C) However, late mature glial cell marker, *olig2*, expression was reduced in *eif2b3* mutants at 3 dpf, especially in the forebrain region (asterisk) and retina (R). (D) Ectopic appearance of microglial progenitor cells in *eif2b3* mutant zebrafish. Earlier detection of neutral red-stained microglial progenitor cells (arrows) on the eye (2 dpf) and midbrain (3 dpf) of *eif2b3* mutant zebrafish compared to WT. (E) Lack of *apoeb*-expressing microglial cells in the midbrain of *eif2b3* mutant zebrafish compared to WT (arrows). Scale bars, 200 μm.

Figure 4

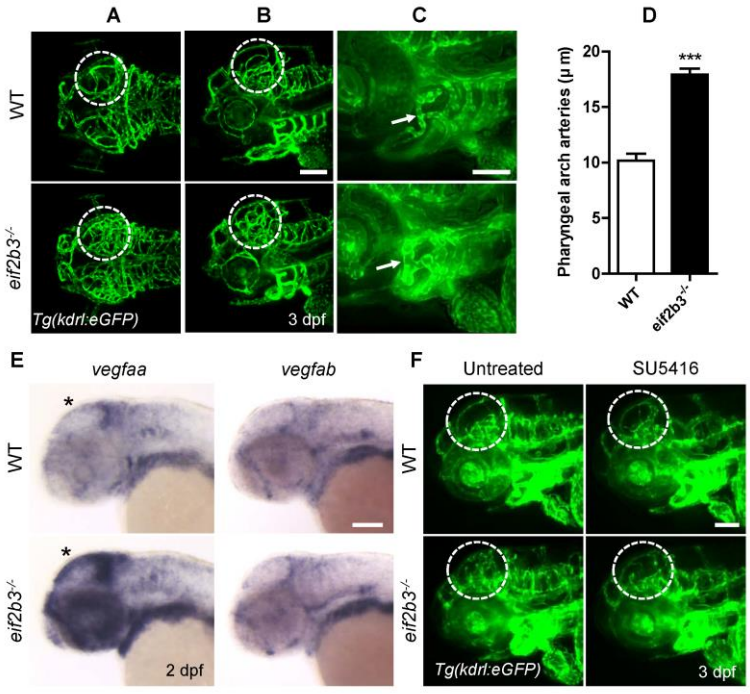

Figure 4. Ectopic angiogenesis in *eif2b3* mutant zebrafish. (A, B) Hyper-branching blood vessels in the midbrain (dotted circle) of *eif2b3* mutant zebrafish crossed with *Tg(kdrl:eGFP)*. (C, D) Increase in blood vessel diameter in *eif2b3* mutant zebrafish compared to WT. (E) Upregulation of *vegfaa* mRNA expression in the midbrain region (asterisk) of *eif2b3* mutants at 2 dpf, compared to WT; however, *vegfab* expression was not significantly changed. (F) VEGFR inhibitor SU5416 inhibits angiogenesis in *eif2b3* KO mutants at 3 dpf. Ventral views (A) and lateral views (B, C, E, F) of cerebral vasculature. Anterior to the left.

Figure 5

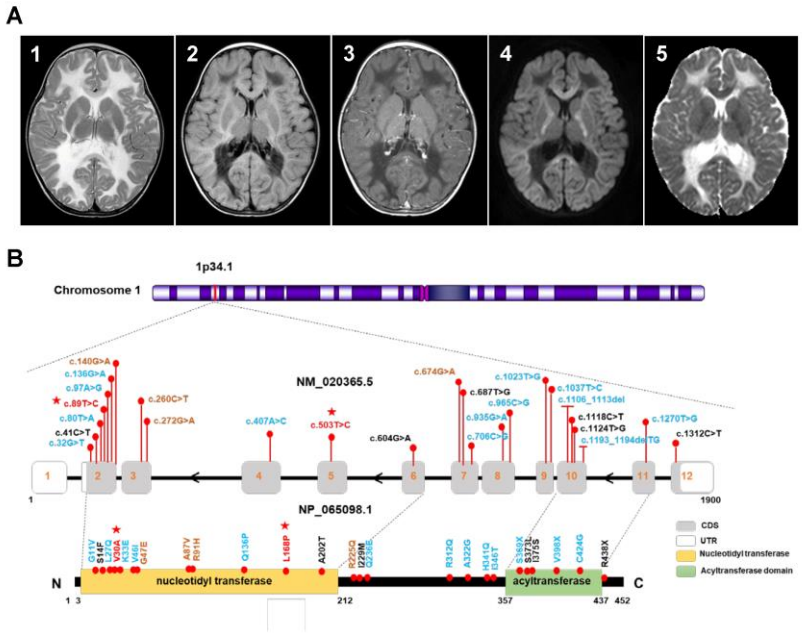

Figure 5. MRI of patient at 19 months of age and schematic of known *EIF2B3* mutations. (A) The axial T2-weighted image (1) shows diffuse T2 hyperintensity of periventricular and deep white matter. The T2 FLAIR image (2) shows hypointense signal of involved white matter similar to CSF. Relative sparing of subcortical U-fibers is seen. Radiating hyperintense stripes in the involved white matter are also observed. Contrast-enhanced T1-weighted image (3) shows hypointensity of involved white matter without contrast enhancement. On the diffusion weighted image (DWI) (4) and apparent diffusion coefficient (ADC) map (5), restricted diffusion is seen in the internal capsule, corpus

callosum, and subcortical white matter. (B) Mutations in *EIF2B3* and domain structure of the protein. Among the reported 25 mutations depicted here, we assessed 19 in zebrafish (the 6 untested mutations are colored in black). The two compound heterozygous mutations found in our patient are colored in red with asterisks. Five additional mutations tested for protein modeling are colored in brown. The longest isoform of NM_020365.5 containing 12 exons is represented by white and gray boxes, which are connected by a horizontal black line representing the introns. The 5'- and 3'-UTRs are depicted by white boxes. Identified mutations on the cDNA level are depicted in red above the exons, while corresponding amino acid changes are listed on the protein level (NP_065098.1) with two functional domains.

Figure 6

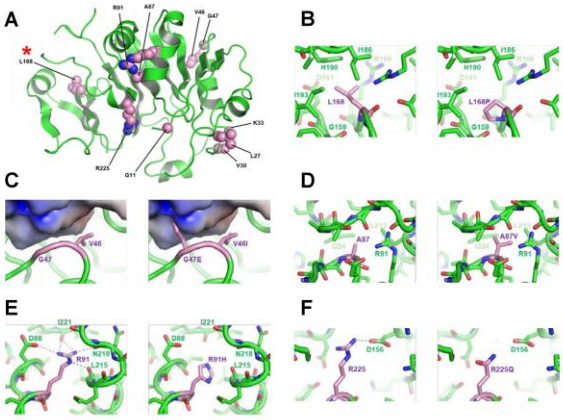

Figure 6. Molecular modeling of EIF2B3 variants and functional validation using *eif2b3* mutant zebrafish model. (A) Side chains of 10 amino acids affected in VWM patients are indicated as spheres. Among them, 4 residues (G11, L27, V30, and K33) are not included because they may adopt uncertain flexible conformations. (B) Interior misfolding due to L168P variation. EIF2B3 mutant L168P (right) are modeled based on wild-type (left) EIF2B3 structure (PDB code 6CAJ). EIF2B3 residues are colored in green except for substituted residues that are presented in violet. Wild-type on the left shows the interaction of L168 with R166 and H190 for proper interior protein folding, whereas the right panel shows the misfolded conformation as L168P loses contact with R166 and H190. The mutation also causes steric hindrance between the C_δ atom of the mutated proline and main chain carbonyl group of G159.

Figure 7

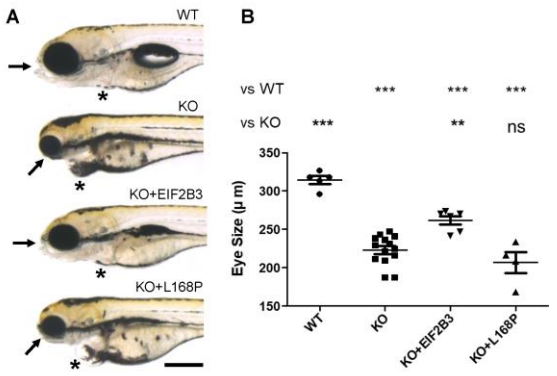

Figure 7. Systematic functional analysis of human EIF2B3 variants using *eif2b3* mutant zebrafish model. 20 expression vectors, including WT EIF2B3 and 19 variants identified from VWM patients were tested in a zebrafish model (Supplementary Material, Figure S5). (A) Synthetic mRNA from each variant expression vector was microinjected into *eif2b3* mutant zebrafish embryos. Representative data for rescue by mutant L168P mRNA (KO+ L168P, *n*= 51) is shown, compared to normal EIF2B3 mRNA (KO+ EIF2B3, *n*= 84). 5 days after microinjection, rescue activity was evaluated by recovery for morphological defects, especially in mouth opening and protruding-mouth (arrows), edema in heart region (asterisks), and eye size (B: eye diameter, μm). $^{**}p < 0.01$, and $^{***}p < 0.001$, unpaired *t*-test. Values are mean±SEM.